Supporting Information

Mulder et al. 10.1073/pnas.0912484106

SI Text

1. Paxinos G, Franklin KBJ (2001) *The Mouse Brain in Stereotaxic Coordinates* (Academic, San Diego, CA).
2. Bons N, et al. (1998) A stereotaxic atlas of the grey lesser mouse lemur brain (*Microcebus murinus*). *Brain Res Bull* 46:1–173.
3. Mulder J, et al. (2009) Tissue profiling of the mammalian central nervous system using human antibody-based proteomics. *Mol Cell Proteomics* 8:1612–1622.
4. Wagner L, et al. (2000) Cloning and expression of secretagogin, a novel neuroendocrine- and pancreatic islet of Langerhans-specific Ca^{2+}-binding protein. *J Biol Chem* 275:24740–24751.
5. Lai M, et al. (2006) Secretagogin, a novel neuroendocrine marker, has a distinct expression pattern from chromogranin A. *Virchows Arch* 449:402–409.
6. Gartner W, et al. (2007) New functional aspects of the neuroendocrine marker secretagogin based on the characterization of its rat homolog. *Am J Physiol Endocrinol Metab* 293:E347–E354.
7. Wyss JM, Sripanidkulchai K (1983) The indusium griseum and anterior hippocampal continuation in the rat. *J Comp Neurol* 219:251–272.
8. Adamek GD, Shipley MT, Sanders MS (1984) The indusium griseum in the mouse: Architecture, Timm's histochemistry and some afferent connections. *Brain Res Bull* 12:657–668.
9. Mody I, Kohr G, Otis TS, Staley KJ (1992) The electrophysiology of dentate gyrus granule cells in whole-cell recordings. *Epilepsy Res Suppl* 7:159–168.
10. Staley KJ, Otis TS, Mody I (1992) Membrane properties of dentate gyrus granule cells: Comparison of sharp microelectrode and whole-cell recordings. *J Neurophysiol* 67:1346–1358.
11. Harkany T, et al. (2003) Complementary distribution of type 1 cannabinoid receptors and vesicular glutamate transporter 3 in basal forebrain suggests input-specific retrograde signalling by cholinergic neurons. *Eur J Neurosci* 18:1979–1992.
12. Riedel A, et al. (2002) Principles of rat subcortical forebrain organization: A study using histological techniques and multiple fluorescence labeling. *J Chem Neuroanat* 23:75–104.
13. Celio MR (1990) Calbindin D-28k and parvalbumin in the rat nervous system. *Neuroscience* 35:375–475.
14. Celio MR, et al. (1988) Monoclonal antibodies directed against the calcium binding protein parvalbumin. *Cell Calcium* 9:81–86.
15. Celio MR, et al. (1990) Monoclonal antibodies directed against the calcium binding protein Calbindin D-28k. *Cell Calcium* 11:599–602.
16. Brumovsky P, Villar MJ, Hokfelt T (2006) Tyrosine hydroxylase is expressed in a subpopulation of small dorsal root ganglion neurons in the adult mouse. *Exp Neurol* 200:153–165.
17. Schwaller B, et al. (1993) Characterization of a polyclonal antiserum against the purified human recombinant calcium binding protein calretinin. *Cell Calcium* 14:639–648.
18. Li ZS, Furness JB (1998) Immunohistochemical localisation of cholinergic markers in putative intrinsic primary afferent neurons of the guinea-pig small intestine. *Cell Tissue Res* 294:35–43.
19. Pike CJ, et al. (1993) Neurodegeneration induced by beta-amyloid peptides in vitro: The role of peptide assembly state. *J Neurosci* 13:1676–1687.
20. Martin-Ibanez R, et al. (2006) Vesicular glutamate transporter 3 (VGLUT3) identifies spatially segregated excitatory terminals in the rat substantia nigra. *Eur J Neurosci* 23:1063–1070.
21. Arita DY, Di Marco GS, Schor N, Casarini DE (2002) Purification and characterization of the active form of tyrosine hydroxylase from mesangial cells in culture. *J Cell Biochem* 87:58–64.
22. Bernier PJ, et al. (2002) Newly generated neurons in the amygdala and adjoining cortex of adult primates. *Proc Natl Acad Sci USA* 99:11464–11469.
23. Mullen RJ, Buck CR, Smith AM (1992) NeuN, a neuronal specific nuclear protein in vertebrates. *Development* 116:201–211.
24. Karlsen AE, et al. (1991) Cloning and primary structure of a human islet isoform of glutamic acid decarboxylase from chromosome 10. *Proc Natl Acad Sci USA* 88:8337–8341.
25. Nagatsuka Y, et al. (2003) Carbohydrate-dependent signaling from the phosphatidylglucoside-based microdomain induces granulocytic differentiation of HL60 cells. *Proc Natl Acad Sci USA* 100:7454–7459.
26. Mikuni N, Babb TL, Chakravarty DN, Chung CK (1998) Postnatal expressions of nonphosphorylated and phosphorylated neurofilament proteins in the rat hippocampus and the Timm-stained mossy fiber pathway. *Brain Res* 811:1–9.
27. Stanic D, et al. (2008) Peptidergic influences on proliferation, migration, and placement of neural progenitors in the adult mouse forebrain. *Proc Natl Acad Sci USA* 105:3610–3615.

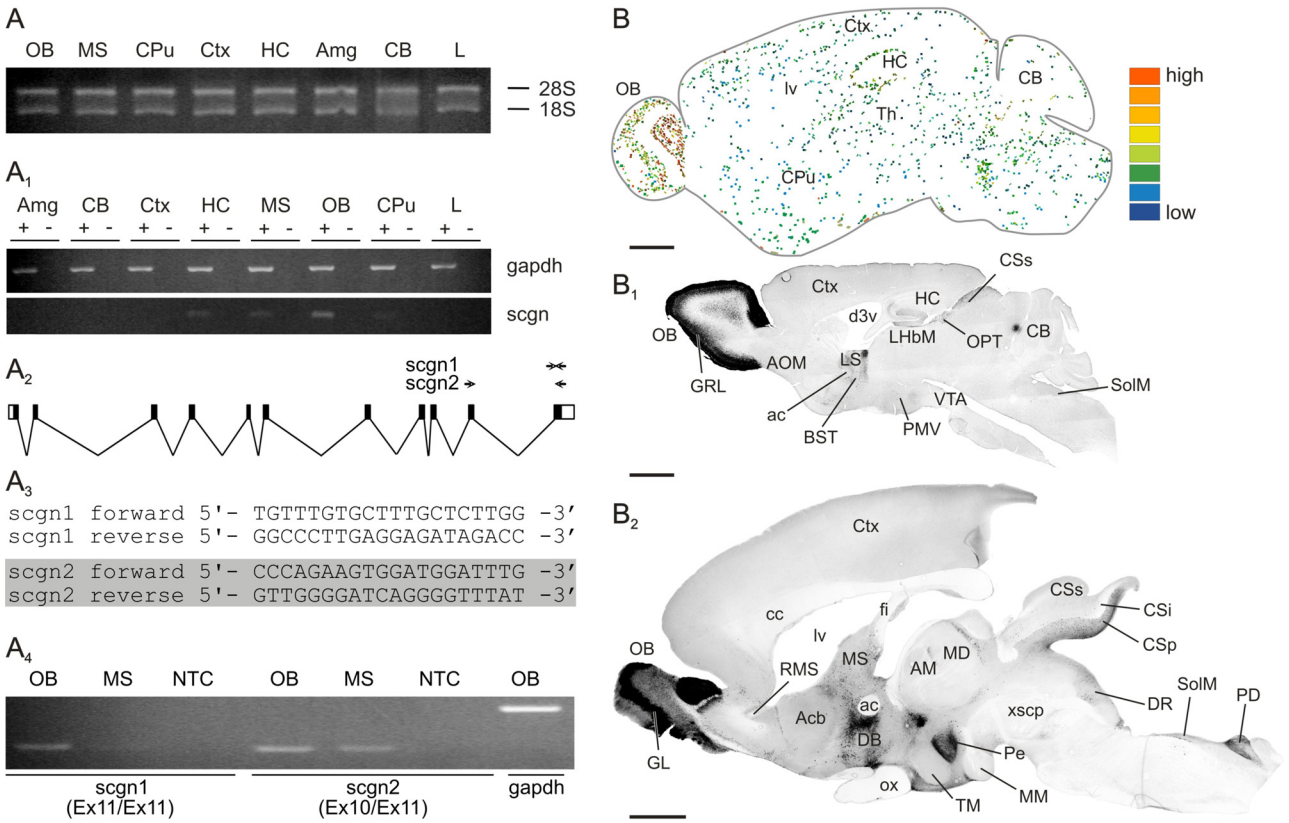

B3

3v	third ventricle
ac	commissura anterior
Acb	nucleus accumbens
AM	anteriodorsal thalamic nucleus
AOM	anterior olfactory nucleus, medial part
BST	bed nucleus of the stria terminalis
CB	cerebellum
cc	corpus callosum
CPu	caudateputamen
CSs	colliculus superior, stratum superficiale
CSi	colliculus superior, stratum intermedium
CSp	colliculus superior, stratum profundum
Ctx	cerebral cortex
d3v	dorsal region of third ventricle
DB	diagonal abnds of Broca
DR	dorsal raphe
fi	fimbria
GL	glomerular layer of the olfactory bulb
GRL	granular cell layer of the olfactory bulb
HC	hippocampus
LHbM	lateral habenular nucleus, medial part
LS	lateral septum
lv	lateral ventricle
MD	mediodorsal thalamic nucleus
MM	medial mammillary nucleus
MS	medial septum
OB	olfactory bulb
OPT	olivary pretectal nucleus
ox	optic chiasm
PD	dorsal paramedian nucleus
Pe	periventricular hypothalamic nucleus
PMV	premammillary nucleus, ventral part
RMS	rostral migratory stream
SolM	nucleus of the solitary tract, medial part
TM	tuberomamillar hypothalamic nucleus
VTA	ventral tegmental area
xscp	decussation of the superior cerebellar peduncle

Fig. S1. Regional and interspecies differences in scgn expression. (*A*) Isolation of intact RNA is essential for gene expression profiling. Therefore, we ran an aliquot of total RNA (1 μg) isolated from microdissected adult mouse brains (RNeasy Mini kit; Qiagen) on a 1.0% agarose gel with GelGreen (Biotium). Sharp 28S and 18S rRNA bands indicate intact total RNA. Liver tissue (L) was used as negative control (see also Fig. 1*A*). (A_1) Real-time qPCRs were validated by preliminary testing of amplification efficacy and by excluding the possibility of genomic DNA contamination in the presence (+) or absence (−) of reverse transcriptase in parallel and running the samples on 1.5% agarose gel. Data for both gapdh, a housekeeping gene used as internal standard, and scgn are shown. (A_2) Exon (Ex, solid squares)/intron (lines) map of the scgn gene. Open squares indicate 5′ and 3′ untranslated regions. Arrows indicate the relative position and orientation of primers used to amplify scgn cDNA by qPCR. (A_2 and A_3) Primer sequences, designed either within Ex11 or in Ex10 (forward) and Ex11 (reverse), used to perform qPCRs. Note that both primer pairs amplify appropriately with primer pair 2 (scgn2, highlighted) providing higher efficacy as demonstrated by an appreciable increase in the amplicon quantity from samples of the olfactory bulb (OB) and medial septum (MS). Data on gapdh is provided as positive control. Abbreviations in A_1–A_4: Amg, amygdala; CB, cerebellum; CPu, caudate putamen; Ctx, cerebral cortex; HC, hippocampus; NTC, nontemplate control. (*B*) scgn in situ hybridization signal from adult mouse brain. A scgn mRNA distribution map available in the Allen brain atlas (www.brain-map.org; image series: 583549) was color coded and modified to optimally visualize olfactory, cortical, and ventral pallidal areas harboring pronounced scgn expression. Colors from blue toward red correspond to incrementing scgn expression levels. (B_1 and B_2) scgn immunoreactivity in sagittal sections of adult mouse (B_1) and gray mouse lemur (B_2) brain. (B_3) List of abbreviations used in B_1 and B_2. [Scale bars, 1 mm (*B* and B_1) and 2.5 mm (B_2).] Nomenclature for mouse and lemur brains was adopted from Paxinos and Franklin (1) and Bons et al. (2), respectively.

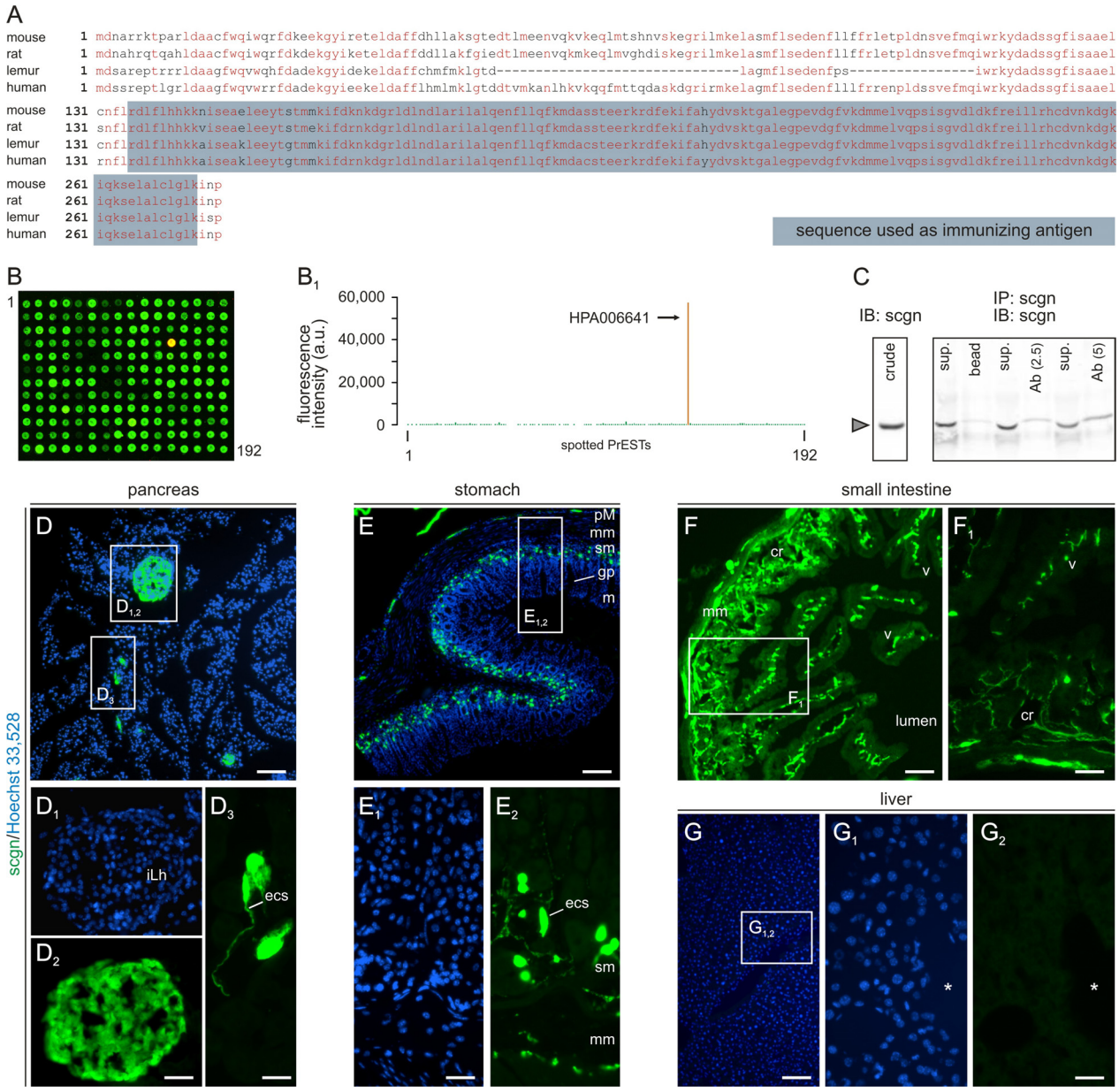

Fig. S2. Antibody validation by scgn expression profiling in neuroendocrine cells of peripheral organs. (*A*) Partial amino acid (aa) sequence alignment of mouse, rat, lemur, and human scgn. Phylogenetically conserved aa residues are shown in red. Gray box indicates a C-terminal sequence used to generate antibodies with high homology across mammals (mouse, 96%; rat, 96%; gray mouse lemur, 99%; as compared to human). (*B* and B_1) Protein array containing 192 protein epitope signature tags (PrESTs) were used for initial screening of antibody specificity. Note that the anti-scgn antibody used in the present study (HPA006641) selectively recognizes its cognate PrEST, while no binding to other peptide fragments present in this protein microarray was detected (3). (*C*) We have further tested the specificity of our antibody by performing immunoprecipitation (IP) experiments. Western blot analysis (IB) of tissue lysates from adult mouse OB revealed a single immunoreactive band at the predicted molecular weight of scgn. We then performed IP without primary antibody (bead) and with incrementing primary antibody concentrations (Ab = 2.5 or 5.0 μL), while keeping the concentration of GammaBind G Sepharose beads (GE Healthcare) used to precipitate the primary Ab constant. Subsequently, membranes were reprobed with scgn primary Ab. Incrementing primary Ab concentrations in IP experiments led to a proportional increase in enriched scgn and, conversely, to a gradual scgn depletion of remnant supernatants (sup.) of whole cell lysates subjected to analysis. These data support that the polyclonal anti-scgn antibody used throughout this report recognizes a single target molecule. (*D*–G_2) scgn has recently been cloned from neuroendocrine organs with highest expression in β cells of the pancreatic islands of Langerhans (iLh) (4) and neuroendocrine cells of other organ systems including the gastrointestinal tract (5, 6). Therefore, we have further validated our anti-scgn antibody by means of high-resolution histochemistry on 16-μm thick cryostat sections of the mouse pancreas (*D*–D_2), stomach (*E*–E_3), and small intestine (*F* and F_1). Liver tissue, lacking appreciable scgn expression (Fig. 1*A*), served as negative control (*G*–G_2). In the pancreas, scgn immunoreactivity revealed β cells of iLh (*D*–D_2) and small clusters of putative endocrine cells (ecs) with often long processes (D_3). (*E*–E_2) In the stomach, scgn immunoreactivity localized in often elongated cells in gastric glands at the base of gastric pits (gp), likely enteroendocrine cells (ecs), and in cells of the plexus of Meissner (pM). (*F* and F_1) Similarly, in the small intestine scgn immunoreactivity is seen in several layers including cells lining the crypts (cr) and the muscularis mucosa (mm). Hoechst 35,528, a nuclear dye, has been applied to reveal tissue architecture. Asterisks in G_1 and G_2 mark blood vessel. m, mucosa; sm, submucosa; v, villi. [Scale bars, 10 μm (D_3), 30 μm (D_2, E_1, F_1, and G_2), and 120 μm (*D*–*G*).]

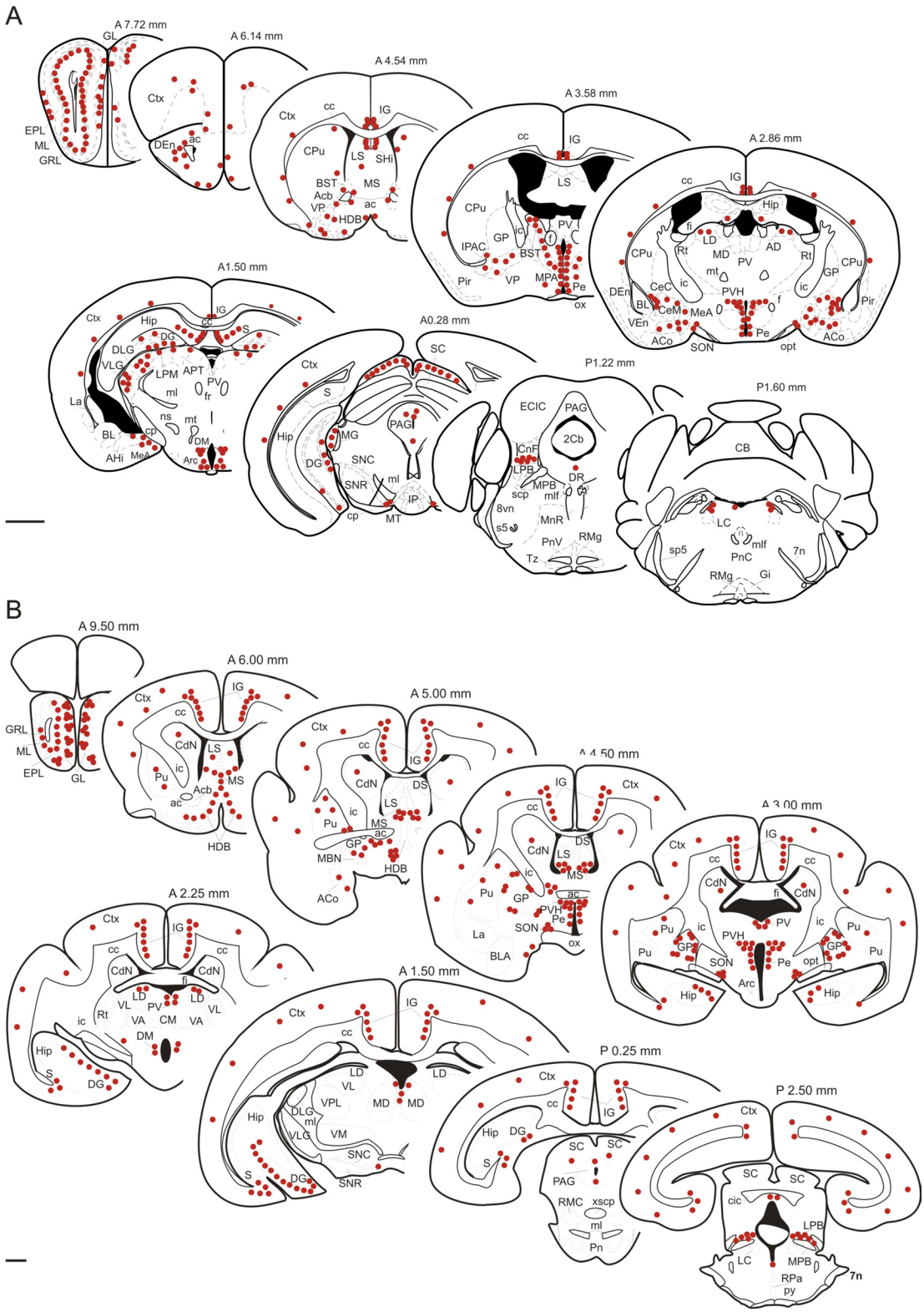

Fig. S3. Distribution of scgn-expressing neurons in rodent and primate brain. Morphometric maps of scgn$^+$ neurons have been assembled by inspecting serial sections of adult mouse (*A*) and gray mouse lemur (*B*) brains (n = 2–5 per species). Solid red circles denote the location of scgn$^+$ neurons. The density of labels alludes to the relative density of scgn$^+$ cells. We have conformed to the nomenclature of Paxinos and Franklin (1) and Bons et al. (2) for mouse and gray mouse lemur brains, respectively. Abbreviations are referred to in Table S1. Semiquantitative assessment of scgn-immunoreactive neuron and axon density in particular brain regions are given in Table S2. [Scale bars, 1 mm.]

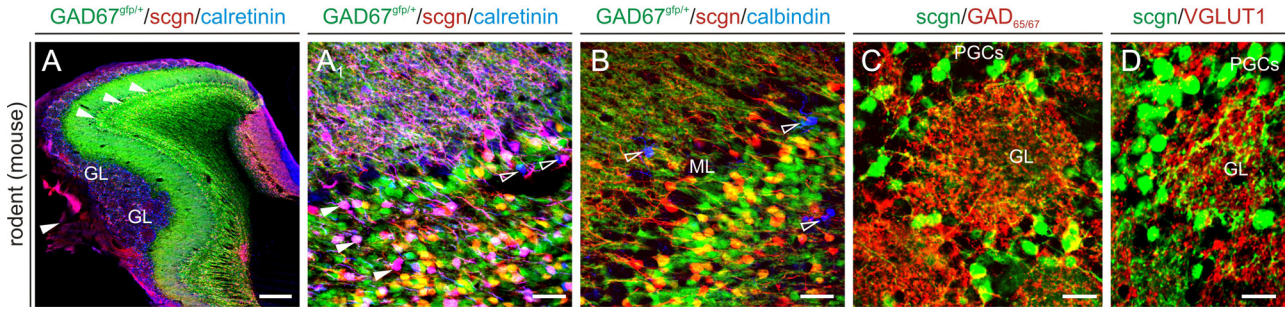

Fig. S4. Identity and synaptic afferents of scgn-expressing neurons in the olfactory bulb of GAD67$^{gfp/+}$ mice. GAD67-GFP (Δneo) mice (GAD67$^{gfp/+}$ mice) were used to explore whether scgn is present in GAD67-expressing neurons. (*A*) GFP signal concentrated in the granule, mitral, and plexiform layers of the OB with a sharp decrease, but not disappearance (see also Fig. 2 D_2 and D_3), in GFP fluorescence in the glomerular layer (GL). Solid arrows indicate the general position of A_1 and *B*. scgn frequently coexists with calretinin in gfp$^+$ neurons (A_1, solid arrowheads) but is excluded from calbindin D28k$^+$/gfp$^-$ Blanes cells (*B*, open arrowheads) in the granular and mitral layers (ML) of the OB. The somatodendritic axis of scgn$^+$ periglomerular cells (PGCs) receives both inhibitory (GAD$_{65/67}^+$, *C*) and excitatory (VGLUT1$^+$, *D*) afferents. [Scale bars, 25 μm (A_1–*D*) and 250 μm (*A*).]

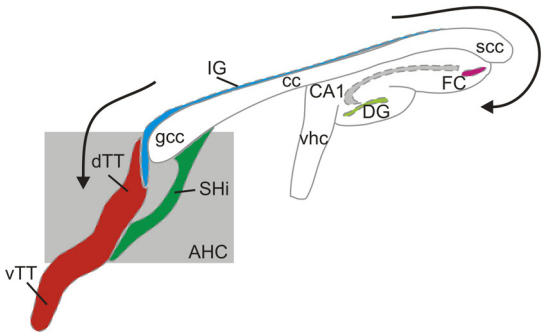

Fig. S5. Topographic organization and spatial relationships of limbic areas containing scgn-expressing granule cells. The dorsal and ventral tenia tecta (d/vTT) form the anterior extremity of a continuum of nuclei containing, among other cell types, neurochemically and cytoarchitecturally similar granule cell-like neurons (7, 8). The vTT is differentiated from the dTT territory by substantial differences in its cell type composition (7). The dTT and its posterior continuation, the septohippocampal nucleus (SHi), show clearly laminated structures with a comprehensive layer of granule cells and thus are cumulatively referred to as the AHC (7). Rostrally, the dTT extends in a mediodorsal direction through a curvature around the genu of corpus callosum (gcc) and its cell mass transits into the IG. The IG is a thin longitudinal supracallosal nucleus extending up until the caudal extremity of the corpus callosum where it folds around the splenium of the corpus callosum (scc) to form the fasciola cinerium (FC) and DG. Arrows indicate major fold directions along the longitudinal axis of the mouse brain. Gray box indicates the general location of cell groups cumulatively classified as AHC (7). CA1, subfield CA1 of the hippocampus; vhc, ventral hippocampal commissure.

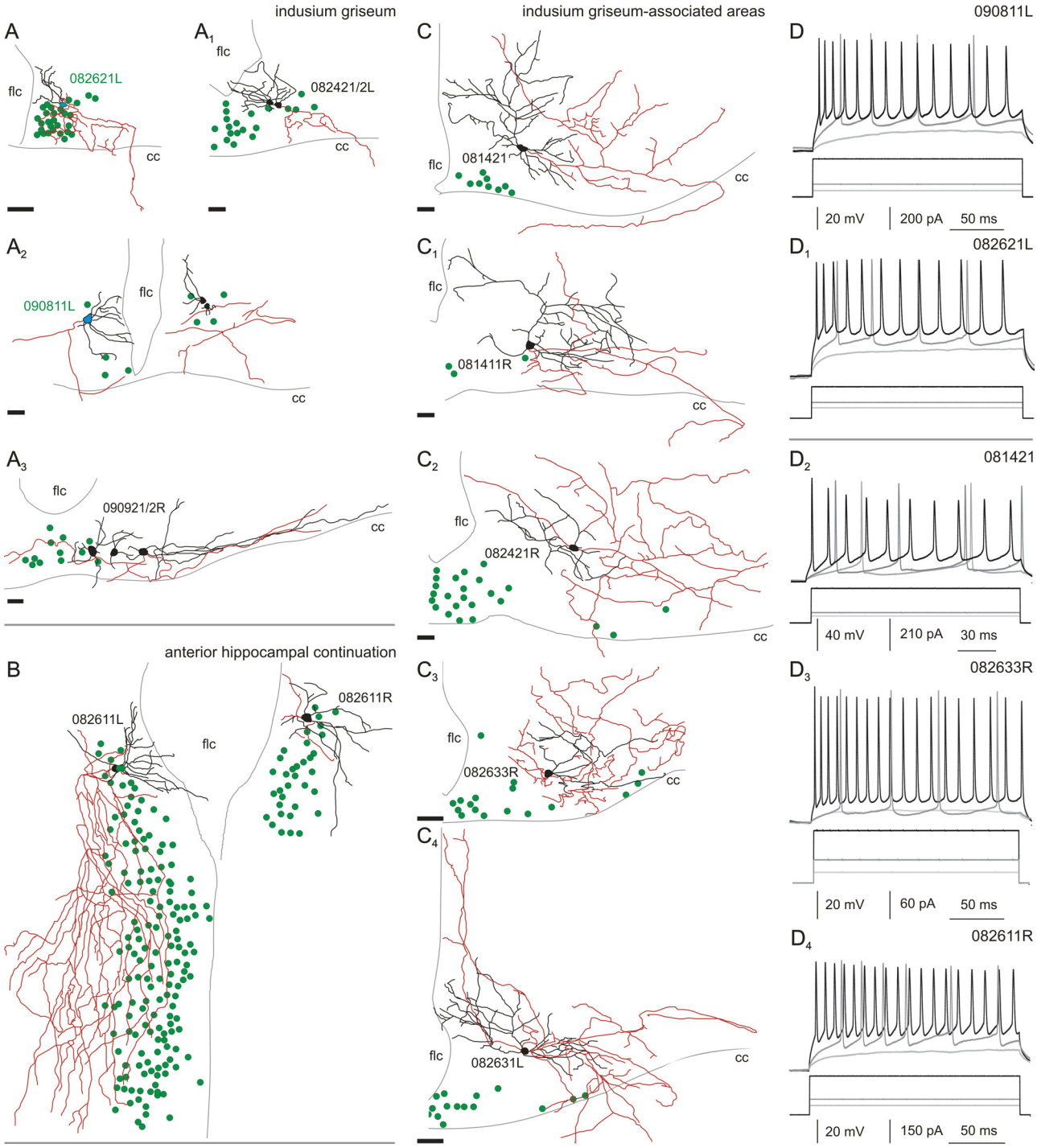

Fig. S6. Neuronal diversity in the IG, neighboring neocortical territories, and anterior hippocampal continuation. (*A*–*C*$_4$) Reconstruction of biocytin-filled neurons was performed after capturing serial images in orthogonal stacks by confocal microscopy. The soma of neurons coexpressing scgn is drawn in blue, whereas that of scgn$^-$ neurons is in black. Dendrites and putative axons are depicted in black and red colors, respectively, in the coronal plane. While the dendritic tree of all cells was largely intact, only local segments of axon collaterals have been traced until the descending axon entered the cc in most cases. Solid green circles indicate the location of scgn$^+$ neurons in relation to reconstructed cells in the indusium griseum (*A*–*A*$_3$), anterior hippocampal continuation (*B*), and neighboring cingulate cortex (*C*–*C*$_4$). Note that cell 082611L was relatively deep in the slice preparation, and although its cytoarchitectonic features correspond to morphological criteria for scgn$^+$ neurons, it remained unstained when using whole slice histochemistry. Solid gray lines are schematic representations of regional and surface boundaries. (*D*–*D*$_4$) Representative whole-cell current clamp records of biocytin-filled neurons. The discharge pattern of scgn$^+$ neurons (*D* and *D*$_1$) is typically characterized by an initial high-frequency action potential (AP) pair followed by adaptation of the AP frequency (see also Fig. 4), and is reminiscent of those seen in dentate granule cells (9, 10). In contrast, AP signatures of scgn$^-$ neurons range from AP frequency and amplitude accommodation (*D*$_2$) to high discharge frequencies (*D*$_3$ and *D*$_4$). flc, fissure longitudinalis cerebri. (Scale bars, 20 μm.)

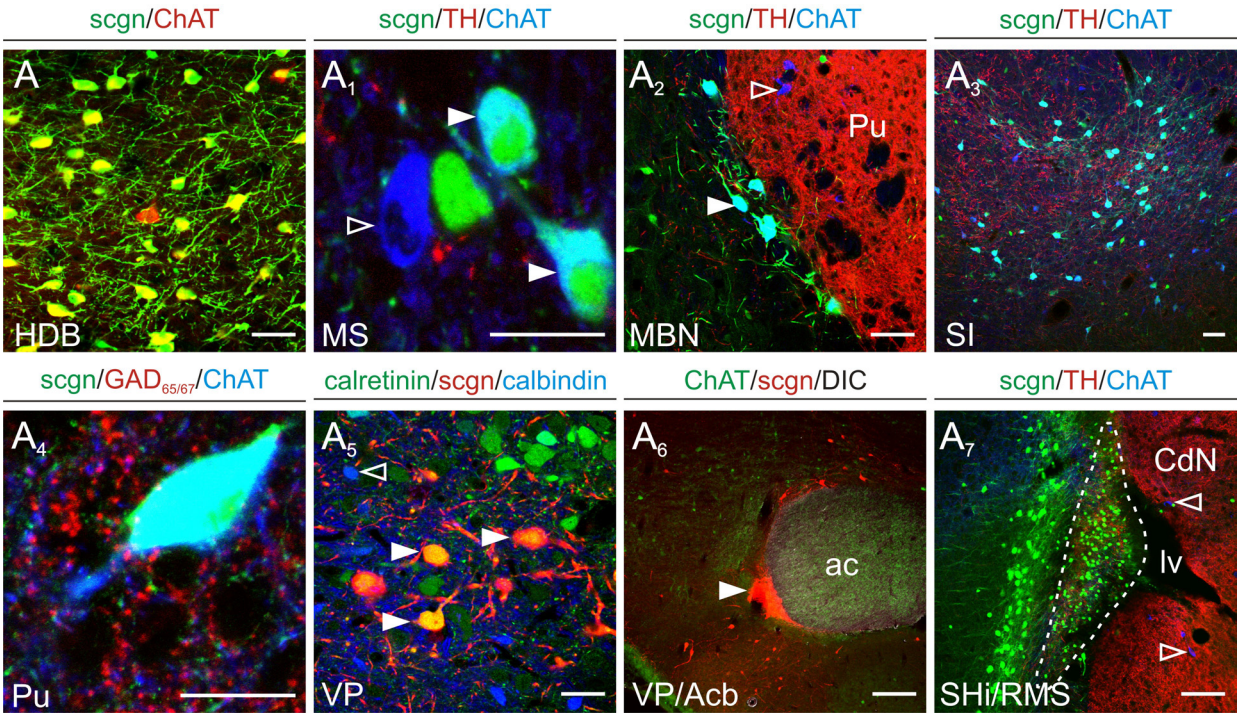

Fig. S7. Scgn expression in basal forebrain territories of the gray mouse lemur. (*A*) Choline-acetyltransferase (ChAT)$^+$ projection neurons of the primate basal forebrain complex, including the horizontal diagonal band of Broca (HDB), express scgn. (A_1) While the majority of cholinergic neurons coexpress ChAT and scgn (solid arrowheads), a proportion (<5%) of cholinergic cells in the medial septum (MS) lack this CBP (open arrowhead). (A_2) Similarly, scgn coexists in cholinergic projection neurons (solid arrowhead) of the magnocellular basal nucleus (MBN). However, scgn is heterogeneously expressed in cholinergic interneurons (open arrowhead)—see also A_4 otherwise—in the nucleus putamen (Pu). (A_3) The dorsomedial substantia innominata contains large scgn$^+$/ChAT$^+$ cholinergic neurons, whereas single labeled scgn$^+$ or ChAT$^+$ cells reside in the laterobasal segment of this area. (A_5) scgn$^+$ neurons coexpress CR (solid arrowheads) but not CB (open arrowhead) in the ventral pallidum (VP). (A_6) Robust scgn immunoreactivity concentrates in the nucleus accumbens (Acb), while a more homogenous distribution of scgn$^+$ neurons is apparent in VP territories. (A_7) scgn is largely absent from cholinergic interneurons (open arrowheads) in the nucleus caudatus (CdN). Note scgn immunoreactivity in the septohippocampal nucleus (SHi) and in rostrally migrating neuroblasts. Dashed line encircles the RMS. ac, anterior commissure; $GAD_{65/67}$, glutamic acid decarboxylase 65/67 kDa isoforms; TH, tyrosine hydroxylase. [Scale bars, 20 μm (A_3), 35 μm (A_1 and A_5), 60 μm (*A*, A_2, and A_4), and 100 μm (A_6 and A_7).]

Other Supporting Information Files

Table S1 (PDF)
Table S2 (PDF)
Table S3 (PDF)